# Autocatalyzed Self-Aggregation of ($3^1R$)-[Et,Et]Bacteriochlorophyll $c_F$ Molecules in Nonpolar Solvents. Analysis of the Kinetics

**Teodor Silviu Balaban,[†] Johannes Leitich, Alfred R. Holzwarth,* and Kurt Schaffner**

*Max-Planck-Institut für Strahlenchemie, Postfach 10 13 65, D-45413 Mülheim an der Ruhr, Germany*

*Received: July 12, 1999; In Final Form: October 28, 1999*

The present work presents a detailed kinetic investigation of the autocatalytic aggregation of ($3^1R$)-[Et,Et]-BChl $c_F$ (BChl *c*) which is the main bacteriochlorophyll contained in the light-harvesting antennae of *Chlorobium tepidum*. Upon dilution with *n*-hexane, solutions of BChl *c* in dichloromethane form the same large aggregates as are encountered in the light-harvesting antennae. These aggregates are characterized by a strongly red-shifted absorption maximum at 739 nm and a tubular structure. The rate of formation of the 739-nm maximum increases dramatically with BChl *c* concentration. The time dependence includes an induction period followed by an exponential buildup and thus results in an overall sigmoidal growth of the aggregate in time. It is evidence in favor of an autocatalytic self-assembly process starting from spontaneously formed critical nuclei, rather than the instant and direct aggregation hitherto assumed for BChl *c*. The empirical equation is presented that describes the buildup of the aggregates in the exponential phase as a function of time and of the overall BChl *c* concentration. Kinetic modeling based on a two-dimensional sheet structure of the 739 nm aggregates (assuming that the tubuli have formed by closure of curved sheets) and on the experimental finding that the 739-nm aggregates have an architecture different from that of the majority of the 680- and 705-nm oligomers that prevail in $CH_2Cl_2$ reproduces this empirical equation. The equation does not discriminate between four formally conceivable two-dimensional patterns of arrangement of the BChl *c* molecules in the sheets, including the one that is strongly favored by already existing experimental and computational evidence. Comparison between the empirical and the kinetically modeled equations yields the size of the critical nuclei as ca. 14 BChl *c* molecules for three (including the one that is strongly favored) of the four possible patterns and as ca. 10 for the fourth one.

## Introduction

The self-assembly of molecules into supramolecular species is common both to natural and to synthetic systems and is a topic of acute interest.[1,2] However, the mechanistic details of this process are usually far from straightforward. The aim of controlling and steering the self-assembly in the hope of obtaining preferentially a desired architecture is currently being addressed.[2d] In the present paper we present a detailed study of the self-assembly of a naturally occurring pigment: ($3^1R$)-[Et,Et]bacteriochlorophyll $c_F$ (BChl $c$[3]).

Green photosynthetic bacteria use for light-harvesting purposes BChl *c*, *d*, or *e*, agglomerated in the core of chlorosomes, which are flat oblong organelles attached to the inner side of the cytoplasmic membrane. BChl *c*, as synthesized in such bacteria, is a mixture of components which differ either by the nature of the alkoxyl residue of the 17-propionic ester or by the homologous substituents at C-8 and C-12; additionally, the configuration of C-$3^1$ may be either (*R*) or (*S*).[4]

The supramolecular organization of BChl in the chlorosomes has been subject to intense study and debate during the last two decades.[5] It is now generally accepted that in the core of the chlorosomes proteins do not play a major role in ligating and orienting the BChl molecules as is the case in the better known chlorophyll antenna complexes (for fascinating recent examples see the LH2 structures of *Rhodopseudomonas acidophila*[6a] and *Rhodospirillum molischianum*[6b]). Rather, a different organizational principle is encountered in the chlorosomes, namely the self-assembly of special BChls into supramolecular aggregates. Numerous spectroscopic studies have shown that properties, such as absorption,[7] fluorescence,[8] energy transfer kinetics,[9] circular dichroism,[10] resonance Raman,[11] FT-IR,[12] and solid state $^{13}C$ NMR,[13] are very similar both for in vitro BChl *c* and *d* aggregates, prepared from BChl solutions by addition of nonpolar solvents (hexane), and for native chlorosomes. The most readily recognizable feature of the chlorosomal-type BChl aggregates is the large red shift of the $Q_y$ absorption band from 667 nm for the monomers to over 739 nm for the aggregates. These in vitro chlorosomal-type

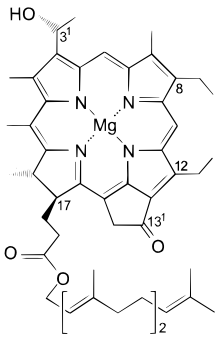


($3^1R$) - [Et,Et]BChl-$c_F$

* To whom correspondence should be addressed. E-mail: Holzwarth@MPI-Muelheim.MPG.De. Fax: (+49)208306395.

[†] Present address: Forschungszentrum Karlsruhe, Institut für Nanotechnologie, D-76021 Karlsruhe, Germany.

10.1021/jp992338p CCC: $19.00 
Published on Web 01/25/2000

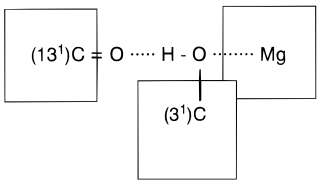


**Figure 1.** Schematic illustration of the bonding network of a type **II** aggregate interconnecting three BChl *c* molecules (symbolized by rectangles) by ligation of the oxygen of one BChl 3¹-hydroxyl to the magnesium of a second BChl with simultaneous hydrogen bonding to the 13¹-keto group of a third BChl.

aggregates possess a tubular structure, the diameters of which Katz and co-workers[14] have determined by neutron small-angle scattering measurements. These diameters are very close to those found by electron microscopy for the BChl rods in the interior of chlorosomes.[15] Experiments with chemically modified BChl compounds have led to the conclusion that the chlorosomal-type aggregates are held together by the bonding scheme outlined in Figure 1. Several two-dimensional architectures as sketched in Figure 15 (vide infra) are *formally* compatible with this bonding scheme (Furthermore, for each of these architectures two versions of maximum symmetry, and more versions of lower symmetry, can exist since since the two sides of the disk-shaped BChl molecules, viewed from their edges in Figure 15, are nonequivalent). Molecular modeling[16] and spectroscopic data[12b,13b] have led us to conclude that architecture **I** (highlighted in Figure 15) is the one that exists in the chlorosomal-type aggregates; the molecular modeling showed, inter alia, that architecture **I** leads to curved two-dimensional sheets which can close to form tubular rods. The predicted rod diameter from our model[16] is in excellent agreement with the experimental data.[14,15] Finally, careful gradual deaggregation experiments, carried out on chlorosomal-type aggregates of BChl *c* and monitored by UV, $^{13}$C-, and $^{1}$H NMR experiments,[17] convincingly support our model of stacks of BChls and moreover indicate that both versions (vide supra) of architecture **I** do coexist.

In chlorinated solvents BChl *c* forms solutions of oligomers which differ quite strongly from the chlorosomal-type aggregates. Olson et al. [18] have reported that complex equilibria exist among these oligomers. Studies with enantiomerically pure components in chlorinated solvents have shown inter alia that different oligomeric species prevail in solution depending on the C-3¹ configuration.[12b] Dilution of BChl *c* solutions in chlorinated solvents with nonpolar solvents (*n*-hexane or a 1:1 (v/v) mixture of *n*-pentane and methylcyclohexane) leads to the formation of chlorosomal-type aggregates (which is the process that we shall investigate in the following). Similarly, larger aggregates, the absorption of which again resembles that of the chlorosomes, form on dilution by water of (monomeric) BChl *c* solutions in lower alcohols; these aggregates have been claimed to form *spontaneously*.[19] According to Amesz and co-workers,[20] BChl *c* on direct dissolution in a 1:1 (v/v) mixture of *n*-pentane and methylcyclohexane at room temperature dissolves to a very low concentration only. These solutions contain two aggregates absorbing at 702 and 719 nm which upon cooling are reversibly converted to (presumably precipitated) larger aggregates with chlorosome-like vis absorption, CD, and fluorescence spectra (Figure 11).

Addition of small amounts of lower alcohols to any BChl *c* solution or suspension converts all aggregates completely to solutions of monomers.[21]

In the present study we show that the formation of the chlorosomal-type aggregates (739-nm absorption) does not occur instantaneously upon dilution of dichloromethane ($CH_2Cl_2$) or 1,1,2,2-tetrachloroethane ($C_2H_2Cl_4$) stock solutions with nonpolar solvents such as *n*-hexane, as has been assumed so far. Rather, the self-assembly is an *autocatalytic* process whereby already formed aggregates catalyze further aggregation. This process starts from spontaneously formed aggregate nuclei.

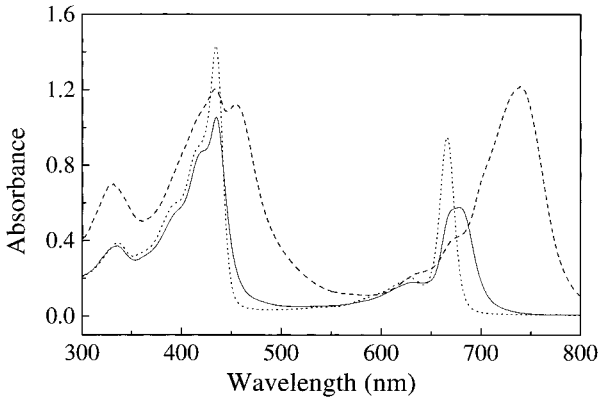


**Figure 2.** Absorption spectra of BChl *c*. Dilute $CH_2Cl_2$ solution (solid line, $c = 14.4\ \mu$M); after adding methanol (dotted line; $CH_2Cl_2$−methanol 95:5 (v/v)). Concentrated $CH_2Cl_2$ solution ($c = 0.12$ mM): after dilution with *n*-hexane (dashed line: $CH_2Cl_2$−*n*-hexane 1:100 (v/v)).

## Experimental Section

*Chlorobium tepidum* was grown anaerobically, and the BChl *c* homologues were isolated as described.[13b] HPLC separation on a Nucleosil-7-C18 reverse-phase column (250 × 20 mm i.d.) by elution with methanol: water (95:5) gave BChl *c* as a main fraction (55%). It was concentrated to dryness in vacuo. Traces of colorless impurities, which had been leaking from the HPLC column, were removed by washing with *n*-hexane. Traces of methanol, which inhibit aggregation, were removed by dissolving the residue in $CH_2Cl_2$ and washing with brine. The organic layer was dried over sodium sulfate and then concentrated in vacuo. The purity of the samples was checked by $^{1}$H- and $^{13}$C NMR and FAB-MS.

Stock solutions of BChl *c* in dry $CH_2Cl_2$ (freshly distilled over calcium hydride) and $C_2H_2Cl_4$ were diluted with dry hydrocarbons such as *n*-hexane by injection of the stock solution into excess hydrocarbon, typically 3.0 mL of *n*-hexane placed in a quartz cuvette of 1 cm path length, and followed by vigorous shaking of the cuvette.

Absorption spectra were measured on a Shimadzu UV-2102 PC scanning and Omega 10 Bruins Instruments spectrophotometers, and CD spectra were recorded on a Jasco J20 instrument.

## Results

**UV-Vis Absorption Spectra.** Figure 2 shows the UV-vis absorption spectra of BChl *c*, the main BChl core constituent of the chlorosomes of *C. tepidum*. The $Q_y$ maximum depends strongly on the solvent and hence on the state of aggregation. In *dilute* solution ($c = 14.4\ \mu$M) in neat $CH_2Cl_2$ a broad band appears around 678 nm, with $\epsilon_{max} \cong 40\ mM^{-1}cm^{-1}$. Addition of methanol causes deaggregation, and the band ultimately sharpens and shifts to 665.5 nm. The absorption coefficient concomitantly increases to $\epsilon_{max} = 66\ mM^{-1}cm^{-1}$, a value which is comparable to that of $\epsilon_{max} = 76\ mM^{-1}cm^{-1}$determined for a mixture of BChl *c* homologues in carbon tetrachloride containing methanol.[22] By contrast, when a concentrated $CH_2Cl_2$ solution of BChl *c* (band maximum at 705 nm) is diluted with a large

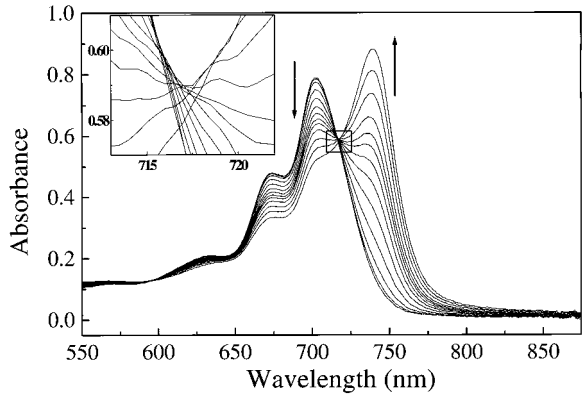


**Figure 3.** $Q_y$ Absorption region at various time intervals after dilution of a $CH_2Cl_2$ stock solution of BChl *c* with *n*-hexane at 293 K (30 $\mu$L of 1.17 mM $CH_2Cl_2$ solution injected into 3 mL of *n*-hexane, i.e., final concentration 11.6 $\mu$M). The cuvette was not removed from the spectophotometer throughout the measurements. Inset: Isosbestic region enlarged.

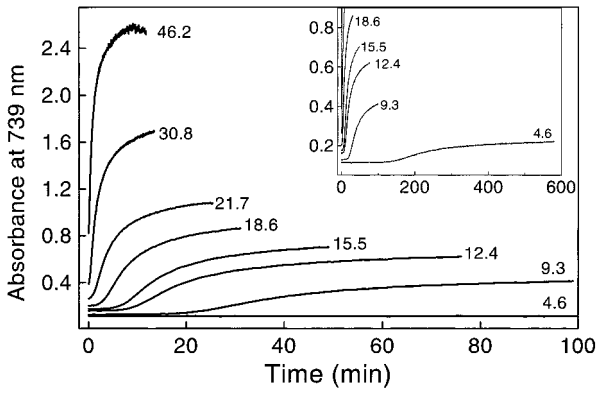


**Figure 4.** Concentration dependence of the rate at which the 739-nm maximum is formed at 298 K. Inset: Time scale extended to 600 min. The numbers on the curves indicate the total BChl *c* concentration ($\mu$M) in the final solutions (*n*-hexane: dichloromethane $\cong$ 80:1). The concentrations of BChl *c* were (from bottom to top): 0.45 mM in $CH_2Cl_2$ diluted to 4.6 $\mu$M in *n*-hexane, 0.85 mM in $CH_2Cl_2$ diluted to 9.3 $\mu$M in *n*-hexane, 1.1 mM in $CH_2Cl_2$ diluted to 12.4 $\mu$M in *n*-hexane, 1.34 mM in $CH_2Cl_2$ diluted to 15.5 $\mu$M in *n*-hexane, 1.57 mM in $CH_2Cl_2$ diluted to 18.6 $\mu$M in *n*-hexane, 1.78 mM in $CH_2Cl_2$ diluted to 21.7 $\mu$M in *n*-hexane; 2.35 mM in $CH_2Cl_2$ diluted to 30.8 $\mu$M in *n*-hexane, 2.56 mM in $CH_2Cl_2$ diluted to 46.2 $\mu$M in *n*-hexane.

excess of *n*-hexane, the $Q_y$ band shifts to an absorption maximum at 739 nm. This red shift can be controlled by a judicious choice of the concentration of the $CH_2Cl_2$ stock solution. In Figure 2 the chlorosome-type $Q_y$ band in *n*-hexane exhibits a small shoulder at about 705 nm, which is due to some remaining oligomers. When the initial concentration of the stock solution is sufficiently high (c $\geq$ 20 $\mu$M) the shoulder is absent.

Figure 3 presents a typical time dependence of the buildup of the 739 nm absorption after dilution of BChl *c* solutions in $CH_2Cl_2$ with *n*-hexane. Note that the decrease of the initial 702-nm maximum and growing-in of the 739-nm absorption proceed without a clean single isosbestic point at around 717 nm. Rather, the transition appears to involve at least two such points. This implies that there is one pair of species involved in the beginning of the aggregation (left point) and an other pair in the final phases (right point); however, even more species may be involved. Figure 4 shows the concentration dependence of the aggregation process. At low BChl concentrations the formation of the 739-nm species is very slow. After an induction period it develops in a sigmoidal time function. Complete aggregation under such conditions takes up to several hours. At higher

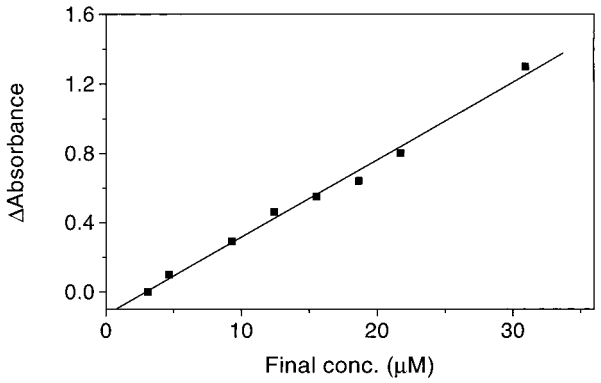


**Figure 5.** Linear dependence on the final BChl *c* concentration of the difference of absorbance at 739 nm between the final and initial states of aggregation as a result of dilution with *n*-hexane.

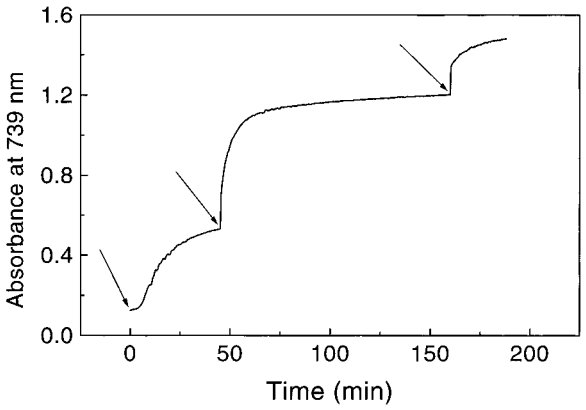


**Figure 6.** Three successive injections (indicated by the arrows) of 1.3 mM solutions of BChl *c* in $CH_2Cl_2$ into 3 mL of *n*-hexane at 293 K. The volumes injected were 30, 50, and 20 $\mu$L, respectively.

concentrations, the 739-nm aggregates form much more rapidly. When close-to-saturated solutions of BChl *c* in $CH_2Cl_2$ are diluted with *n*-hexane, the shift to 739 nm is almost instantaneous on the time scale of our mixing and measuring experiment (i.e., it occurs within seconds), and no 705-nm species can be observed. This overall behavior, in particular the sigmoidal feature, is typical for an autocatalytic aggregation. Figure 5 demonstrates the proportionality of the final 739-nm absorption with total [BChl *c*] in the final *n*-hexane solution ([$\mathbf{B}_{tot}$]).

Once the induction period is over, successive injections of $CH_2Cl_2$ solutions of BChl *c* lead to an *immediate* increase of the absorption maximum at 739 nm, without a sigmoidal feature (Figure 6). This means that the aggregation proceeds smoothly once enough of the 739-nm species is present.

The temperature dependence of the aggregation for a given BChl concentration is shown in Figure 7. The formation of the 739-nm maximum is more rapid at lower temperatures. The descending branch in the curve at 283 K is due to the eventual formation of precipitates in the cuvette at that high concentrazion.

The composition as a function of concentration in *n*-hexane after diluting $C_2H_2Cl_4$ solutions,[23] always at the same short time interval well before completion of the aggregation process, is shown in Figure 8. The ratio of the band areas at 738 and 704 nm obtained by a Gaussian deconvolution exhibits a sigmoidal dependence (inset in Figure 8), which mirrors the sigmoidal dependence obtained in the time domain.

It is of interest to note that, some time after aggregation is completed, a thin film deposits on the cuvette walls when the total BChl *c* concentration is low, and fluff-like material

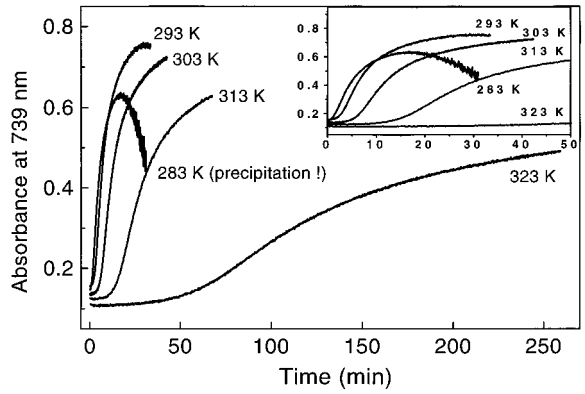


**Figure 7.** Temperature dependence of the formation of the 739-nm maximum of 1.34-mM solutions of BChl *c* in $CH_2Cl_2$ diluted to 15.5 $\mu$M in *n*-hexane. Note that precipitates were formed soon after injection at 283 K. The inset is an expansion of the first 50 min.

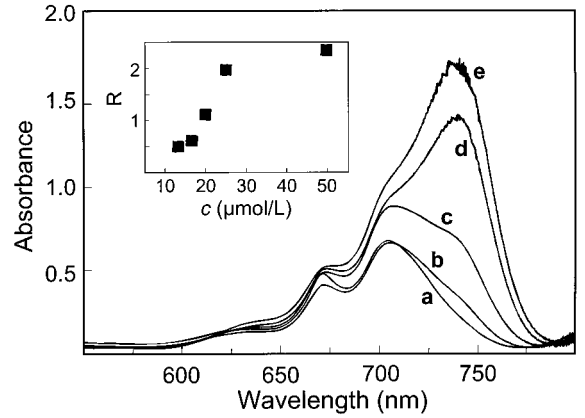


**Figure 8.** Concentration dependence of the $Q_y$ absorption of BChl *c* at 2 min after dilution of $C_2H_2Cl_4$ solutions ($c$ = 2.0, 2.5, 3.0, 3.75, and 7.4 mM) with *n*-hexane; final concentrations a−e in *n*-hexane: 13.2, 16.5, 19.8, 24.8, and 49.6 $\mu$M, respectively. Inset: Ratio $R$ of the 738- and 704-nm band areas (obtained by Gaussian band decomposition), also at 2 min after dilution, as a function of the final concentration.

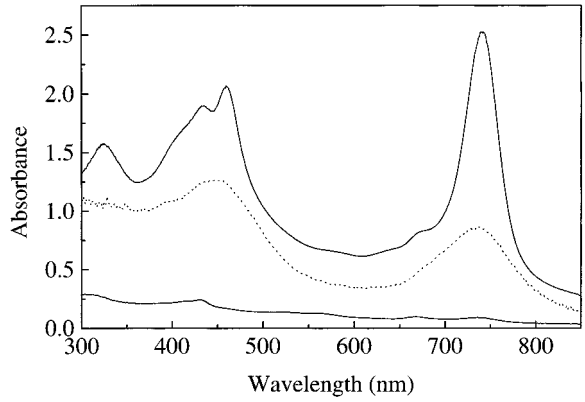


**Figure 9.** Absorption spectra: − −, film on the cuvette wall deposited from a dilute $CH_2Cl_2$ stock solution of BChl *c* upon further dilution with *n*-hexane; (absorbance exaggerated 8-fold); —, (bottom) supernatant of a heterogeneous sample containing fluff-like particles formed upon dilution of a concentrated $CH_2Cl_2$ stock solution with *n*-hexane and standing for several hours (bottom), and (top) homogeneous phase produced by shaking of the heterogeneous sample. The two full-line spectra were recorded for the same sample in the same cuvette.

precipitates when it is high. The absorption maximum of the film deposit is also at 739 nm (Figure 9). This film is insoluble in *n*-hexane, but it is soluble in methanol and thus can be quantified. After a sufficiently long period (up to hours) almost

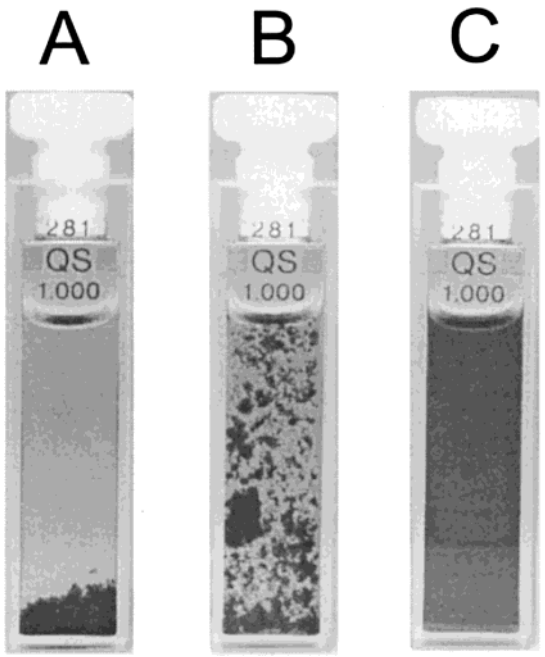


**Figure 10.** Cuvette with BChl *c* aggregates formed upon dilution of a concentrated $CH_2Cl_2$ solution with *n*-hexane: (A) Deposit of macroscopic aggregates of micelles on the bottom of the cuvette after standing for several hours (for the spectrum of the supernatant see bottom full line spectrum in Figure 9). (B) Micelles floating about due to convection upon gentle heating of the bottom of cuvette A; note the almost colorless supernatant in A and B. (C) Homogeneously colored sample obtained by shaking cuvette B vigorously (for the spectrum see top full line in Figure 9).

all BChl *c* is deposited in the film, and the supernatant *n*-hexane phase is practically depleted of BChl *c*.

When the concentration in *n*-hexane exceeds ~40 $\mu$M, the aggregate absorbing at 739 nm precipitates in the form of visible green fluffs, which agglomerate further and are deposited at the bottom. Again, the delay for the appearance of the fluffs shortens with increasing BChl *c* concentration. No film is formed on the cuvette walls under these conditions. After several hours the supernatant *n*-hexane layer is completely depleted of the 739-nm aggregates. The liquid phase has turned colorless and its absorption spectrum is reduced practically to the base line (Figure 9, lower full trace). Shaking of the cuvette or short and mild sonication disrupts the fluffs (Figure 10: step B to C). They are no longer visible by eye, the solution has regained its original greenish-yellow color, and the absorption spectrum now shows again a prominent maximum at 739 nm (Figure 9, upper full trace). On further standing the fluffs reappear. Figures 10A−C illustrate this sequence of events. It can be repeated at will, the aggregates being stable for months, even in daylight, when kept under exclusion of humidity and anaerobic. The results obtained by Amesz and co-workers[20] (vide supra) which we reproduced (Figure 11) suggest an insolubility (under equilibrium conditions) of the 739-nm agregates in nonpolar solvents such as *n*-hexane.

*It is important to note here* that this insolubility does not preclude the kinetic modeling of the formation of the 739-nm aggregates that we shall carry out in the following: First, we shall model only the initial phases of the aggregation process; the initial aggregate fragments will be dissolved (note that the actual precipitation of the final tubular aggregates is a very slow process as compared to aggregate formation). Second, the aggregation proceeds virtually to completion which means there

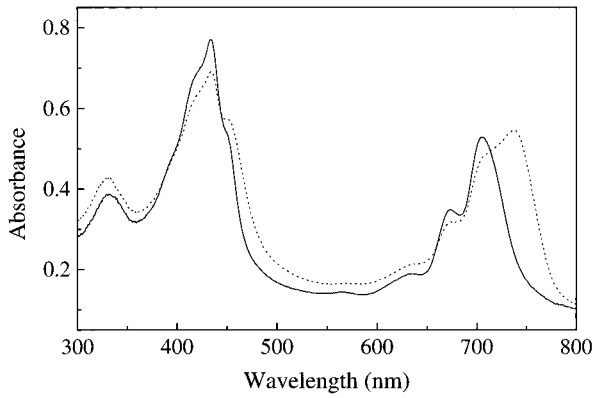


**Figure 11.** Absorption spectra of BChl *c* in *n*-pentane-methylcyclohexane 1:1 (v/v) at 293 K. —, Sample directly dissolved in the mixture of the hydrocarbon solvents; — —, sample dissolved first in $CH_2Cl_2$ then diluted with a large excess of the hydrocarbon mixture.

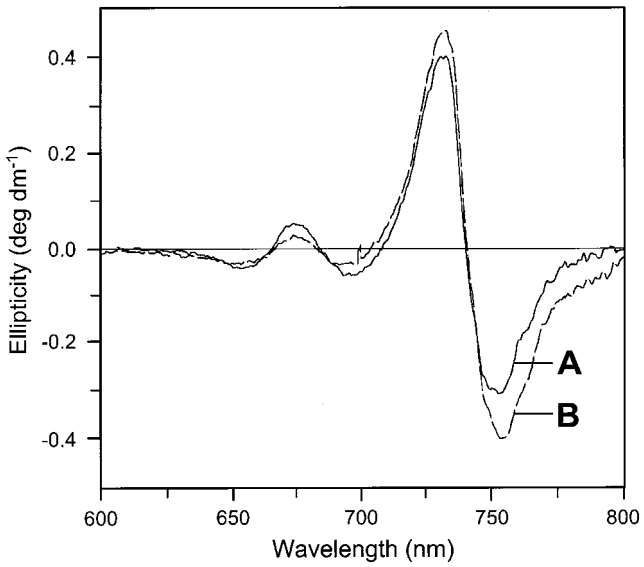


**Figure 12.** CD Spectra in the $Q_y$ region of BChl *c* dissolved in $CH_2Cl_2$ ([BChl *c*] = 0.87 mM) then diluted with *n*-hexane ([BChl *c*] = 8.7 $\mu$M): A, 10 min after dilution; B, ca. 1 h after dilution.

is no competing de-aggregation reaction of the final aggregates (the velocity of which would depend on the state of dissolution).

**Circular Dichroism.** The dilution with *n*-hexane can also be monitored by CD. However, the relatively long scanning times did not permit to acquire more than two CD curves before the self-assembly was completed. Figure 12 shows two CD traces at different time intervals after injection of a $CH_2Cl_2$ stock solution of BChl *c* into *n*-hexane. There are two excitonic couplets: a very intense one with a peak at 730 nm and a trough at 753 nm, which increases with time and is attributed to the 739-nm aggregate, and another one of much weaker intensity with the extrema at 673 and 695 nm, which decreases concomitantly and is assigned to the 680-nm species.

We have presented recently the CD spectra of the C-3[1] epimers of [Et,Me]BChl $c_S$.[10c] In $CH_2Cl_2$ they depend strongly on the configuration and concentration. Upon dilution with *n*-hexane chlorosome-like spectra were obtained for all samples. The 705-nm absorption maximum still dominated 10 min after injection, and it exhibited merely a shoulder at 739 nm. However, the augmented rotatory strength of the 739-nm aggregate caused its CD to prevail already at this point in time. The strong exciton coupling of the chromophores in the 739-nm aggregate determines, of course, the striking characteristics of this signal.

## Aggregation Kinetics

The present work investigates the formation of chlorosomal-type aggregates (**H** (high)) of BChl *c* from oligomers ( **L** (low)) upon dilution of $CH_2Cl_2$ solutions of the latter with saturated hydrocarbons such as *n*-hexane. Figure 4 displays the buildup of **H** (as monitored by the absorbance at 739 nm which is almost entirely due to **H**) with time as a function of the overall BChl *c* concentration in the resulting solutions ($[\mathbf{B}_{tot}]$). Figure 4 immediately reveals one striking feature: namely, the onset of the buildup of **H** is retarded by an induction period. This results in a sigmoid shape of the **H** buildup curves, i.e., the induction period is followed by a steep ascent which then reaches an inflection point after which the buildup levels off again in approach to the final state when virtually all BChl *c* is present as **H**. An induction period is characteristic of autocatalysis; i.e., the **H** already formed induces the further buildup of **H**. This interpretation predicts two phenomena, both of which are observed experimentally: (1) When further **L** (BChl *c* dissolved in a small amount of $CH_2Cl_2$) is added to solutions of BChl *c* in $CH_2Cl_2$/hexane which have reached steady-state concentrations of **H**, and thus the formation of more **H** is induced, this additional **H** is formed without any induction period (Figure 6). (2) The lower $[\mathbf{B}_{tot}]$, the longer the induction period (Figure 4).

Sigmoid buildup curves, superficially quite similar to the ones that we describe here, have been observed before in the course of the self-aggregation of other large biomolecules.[24−26] Invariably, the explanation of these curves[24,26] required an autocatalytic aggregation mechanism and hence required the spontaneous formation of a "critical" aggregation nucleus which exists in very small relative concentration in rapid equilibrium with monomers and oligomers and from which the larger aggregates grow. This situation is quite reminiscent of first-order phase transitions such as crystallization.[27] "Faulty" attachment of a monomer or oligomer to a growing aggregate will be corrected since the misfitted unit will rapidly leave the aggregate again.[28] The relative slowness of the buildup in the present case is also striking: As Figure 4 shows, it takes many minutes up to a few hours, which contrasts to the virtually instantaneous establishment of the equilibria between the various oligomers **L** when $[\mathbf{B}_{tot}]$ in $CH_2Cl_2$ is changed by dilution. This suggests that the critical aggregation nucleus must indeed have a very low equilibrium concentration in company with the oligomers **L**.

Another striking feature is revealed by Figure 7: The buildup rate of **H** decreases with temperature. In terms of the Eyring equation for this rate, viz., $\log k_{obs} = \log(k_B T/h) - \Delta H^{\ddagger}_{obs}/RT + \Delta S^{\ddagger}_{obs}/R$, the inverse temperature dependence implies a negative $\Delta H^{\ddagger}_{obs}$ value and also, since $\log k_{obs} \ll \log(k_B T/h)$, a strongly negative $\Delta S^{\ddagger}_{obs}$ value. The minimal kinetic model for any overall reaction A → C showing a negative $\Delta H^{\ddagger}_{obs}$ value, but composed entirely of elementary reactions that all have positive $\Delta H^{\ddagger}$ values, is

$$\mathrm{A} \underset{k_2}{\overset{k_1}{\rightleftharpoons}} \mathrm{B} \underset{k_4}{\overset{k_3}{\rightleftharpoons}} \mathrm{C}$$

where four independent conditions have to be met:

$$\Delta H^{\ddagger}_2 > \Delta H^{\ddagger}_1 + \Delta H^{\ddagger}_3 \quad (1)$$

$$T(\Delta S^{\ddagger}_2 - \Delta S^{\ddagger}_1) \gg \Delta H^{\ddagger}_2 - \Delta H^{\ddagger}_1 \quad (2)$$

$$T(\Delta S^{\ddagger}_2 - \Delta S^{\ddagger}_3) \gg \Delta H^{\ddagger}_2 - \Delta H^{\ddagger}_3 \quad (3)$$

$$T(\Delta S^{\ddagger}_3 - \Delta S^{\ddagger}_4) \gg \Delta H^{\ddagger}_3 - \Delta H^{\ddagger}_4 \quad (4)$$

**TABLE 1. Fitting of Selected Regimes from the Curves in Figure 4 to Equation 1**

| $[\mathbf{B_{tot}}]$ ($\mu$M)[a] | $t_{low}$ (min)[b] {absorbance} | $t_{high}$ (min)[c] {absorbance} | $N$[a] | $10^4 c$[e] ($cm^{-1}$) | $10^3 d$[f] ($cm^{-1}$) | $s$[g] ($min^{-1}$) |
|---|---|---|---|---|---|---|
| 30.8 | 0.03 {0.387} | 0.47 {0.545} | 14 | 967 ± 98 | 282 ± 11 | 2.1413 ± 0.136 |
| 21.7 | 0.17 {0.263} | 1.67 {0.359} | 10 | 196 ± 21 | 239 ± 3 | 1.0881 ± 0.056 |
| 18.6 | 1.0 {0.206} | 4.33 {0.303} | 11 | 58 ± 11 | 190 ± 3 | 0.6868 ±0.050 |
| 15.5 | 3.0 {0.176} | 10.0 {0.273} | 8 | 13 ± 2.2 | 170 ± 2 | 0.4382 ± 0.022 |
| 15.5 | 2.0 {0.195} | 7.5 {0.314} | 12 | 67 ± 8.6 | 178 ± 3 | 0.4032 ± 0.020 |
| 12.4 | 6.0 {0.165} | 15.0 {0.290} | 10 | 93 ± 32 | 130 ± 11 | 0.1913 ±0.019 |
| 9.3 | 17.0 {0.133} | 27.0 {0.178} | 11 | 10 ± 2.7 | 119 ± 2 | 0.1494 ± 0.012 |
| 4.6 | 99.0 {0.117} | 169.0 {0.134} | 71 | 1.4 ± 0.5 | 112 ± 1 | 0.0301 ± 0.003 |

[a] Overall BChl *c* concentration in the resulting *n*-hexane solutions. [b] Lower bound of selected regime; time (min) after *n*-hexane addition and absorbance at 739 nm at that time. [c] Upper bound; as with footnote b. [d] Number of data points within the regime. [e] $c \equiv \epsilon_{739}(k_h/2)(k_i k_j)^{-1/2}[\mathbf{M}]^{3m/2-1} p_r q_r \exp(-st_r)$. [f] $d \equiv \epsilon_{739}\{[\mathbf{B_H}]_r - (k_h/2)(k_i k_j)^{-1/2}[\mathbf{M}]^{3m/2-1} p_r q_r\}$. [g] $s \equiv 2(k_i k_j)^{1/2}[\mathbf{M}]^{m/2+1}$.

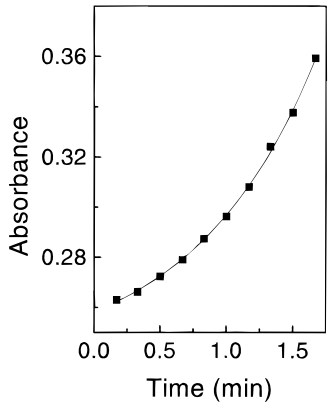


**Figure 13.** Exponential growth of the absorbance (739 nm) of a BChl *c* solution (total final concentration $[\mathbf{B_{tot}}] = 21\ 7\ \mu M$) prepared by diluting a solution in dichloromethane by *n*-hexane. Time of diluting = 0.0 min.

Conditions 2 and 3 make $k_2$ fast relative to $k_1$ and $k_3$, respectively; condition 2 thus implies a quasi-stationary concentration of B that is negligibly small relative to A. Condition 4 renders the reaction step $k_3$ irreversible. Together, these conditions imply that $k_{obs} = k_1 k_3 / k_2$. Condition 1 then provides the negative $\Delta H^{\ddagger}_{obs}$ value. In terms of this minimal model, $\Delta H^{\ddagger}_{obs}$ and $\Delta S^{\ddagger}_{obs}$ can be equated to $\Delta H^0_{f(BC)} - \Delta H^0_{f(A)}$ and $\Delta S^0_{(BC)} - \Delta S^0_{(A)}$, respectively, where A and BC refer to species A and to the transition state between B and C, respectively. Thus, the transition state between B and C is lower both in heat (enthalpy) of formation and in entropy of formation than A since both $\Delta H^{\ddagger}_{obs}$ and $\Delta S^{\ddagger}_{obs}$ are negative. Grossly oversimplified though this minimal kinetic model is in view of the complexity of the actual aggregation process, it does show how the exothermicity of the aggregation process and the entropy decrease caused by the very aggregation may conspire to produce the observed negative activation energy. B may be equated to the above-mentioned critical nucleus of the autocatalytic aggregation process.

Analyzing the sigmoid buildup curves in our system, we shall focus on the early rapid buildup phase after the induction period, well before the inflection point where growth starts to slow. We find that for all but one of the curves in Figure 4 a regime of clean exponential growth can be identified in this phase; in the case of the highest $[\mathbf{B_{tot}}]$ (46.2 $\mu$M), no regime containing a reasonable number of data points could be selected as the buildup was too fast and the inflection point was reached too early after mixing. Figure 13 shows the result of exponential fitting within the regime for $[\mathbf{B_{tot}}] = 21.7\ \mu M$; in the other seven cases the result was similar. We can therefore write for the dependence of aggregate absorbance at 739 nm, $A$, on time $t$ *within the regime*

$$A = c \exp(st) + d \tag{1}$$

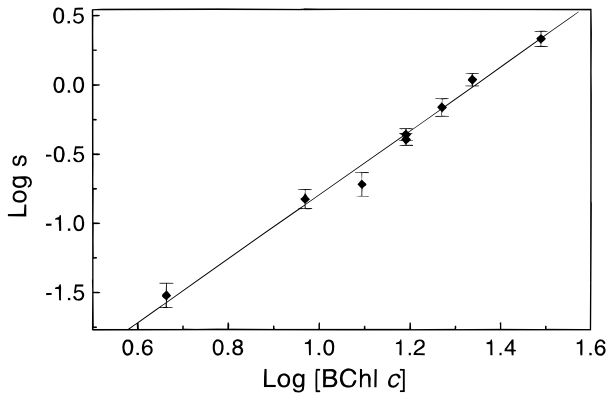


**Figure 14.** Linear dependence of log(s) on log$[\mathbf{B_{tot}}]$ (cf. Table 1).

Table 1 shows the values for $c$, $d$, and s ($\pm\sigma$), produced by the fitting procedure for every single $[\mathbf{B_{tot}}]$.

A plot of the values for log($s$) thus obtained vs log$[\mathbf{B_{tot}}]$ is found to be linear ($r^2 = 0.99$; Figure 14) with a slope of 2.31 ± 0.10.

The quantity s can thus be written as $s = (8.53 \pm 0.24) \times 10^{-4}[\mathbf{B_{tot}}]^{(2.31 \pm 0.1)}$. On scrutiny of the values for $c$ we note some "roughness" in the growth of $c$ with $[\mathbf{B_{tot}}]$. This must be due to experimental problems as is strikingly revealed by the two values for $c$ at $[\mathbf{B_{tot}}] = 15.5\ \mu M$ which diverge quite strongly. Since, by contrast, the two pairs of values for d and s at the same concentration show good mutual agreement it is clear that the experimental problem must reside with the correct determination of the time zero of the aggregation reaction, which determines $c$ and which carries some uncertainty. Nevertheless, a linear plot according to $\log c = a_0 + a_1 \log[\mathbf{B_{tot}}]$, using all $c$ values, shows an acceptable correlation ($r^2 = 0.827$) and yields $a_0 = -6.00 \pm 0.45$ and $a_1 = 3.17 \pm 0.39$. These relationships can now be compounded into the empirical expressions 2 and 3 describing the buildup of aggregate absorption at 739 nm within said regimes, *i.e.*, well after the induction period and well before the inflection point:

$$A = [\mathbf{B_H}]\epsilon_{739} = 10^{-(6 \pm 0.45)}[\mathbf{B_{tot}}]^{(3.17 \pm 0.39)} \exp(st) + d \tag{2}$$

where $[\mathbf{B_H}]$ is the concentration of BChl $c$ that is bound in 739 nm aggregates,

$$s = (8.53 \pm 0.24) \times 10^{-4}[\mathbf{B_{tot}}]^{(2.31 \pm 0.1)} \tag{3}$$

and $d$ as given in Table 1

($[\mathbf{B_H}]\epsilon_{739}$ in $cm^{-1}$, $[\mathbf{B_{tot}}]$ in $\mu$M, $t$ in min)

### Modeling of the Aggregation Kinetics

We may now compare the system studied in the present work with other systems that also show a sigmoid buildup. An intensively studied example is that of deoxyhemoglobin S.[24] For this system, in the early time regime of the aggregation but after the induction period, an exponential growth law was found, just as we find here for BChl *c*. However, a dependence between log(s) and the logarithm of concentration was found there that was much more complicated than the linear dependence that we find here. The kinetic rate law which excellently reproduced this complicated dependence had been derived from a mechanistic model based on the structure of the deoxyhemoglobin S aggregate. This structure, a compact rod that resembles a 14-stringed braid, is quite different from the tubular structure of the BChl *c* aggregates which we consider here, whatever the detailed architecture of the tubular structure may be. Thus, while the overall sigmoid appearance of buildup curves may be common to all autocatalytic mechanisms that involve nucleation, the concentration dependence of the curves and the mechanistic model describing this dependence specifically relate to the architecture of the aggregate, as may have been expected. Not even the exponential time dependence in said regimes can be taken as general since we find, e.g., a third-power dependence in its place for one (obviously faulty) structural and kinetic model (not discussed in this paper) for the BChl *c* tubular aggregate. This situation suggests a possibility to verify or reject a structural model for the BChl *c* tubular aggregate by exploring whether a kinetic model implied by the structural model leads to equations that agree or are at variance with experiment. As the following modeling will show, the observed aggregation kinetics confirm the two-dimensional sheet structure of the aggregates (note that the tubuli are curved sheets that have closed to form a tube) and moreover confirm that their architecture is different from that of the oligomers present in chlorinated hydrocarbons. They do not discriminate between four conceivable architectures (**I**−**IV**) of the sheets which are sketched in Figure 15 and which agree with the bonding scheme of Figure 1, but they still yield the approximate size of the critical nucleus.

Of the four formally conceivable architectures (**I** − **IV**, Figure 15) that comply with Figure 1, **I** (highlighted in Figure 15) is the one that is strongly favored by the available experimental and computational evidence (vide supra, Introduction section) whereas **III** and **IV** are the so-called parallel and antiparallel chain models, respectively, proposed by Brune, King, and Blankenship.[29] We have also included **II**−**IV** in the kinetic modeling since formally the modeling will not discriminate between them. All four architectures can be represented by the general structure given also in Figure 15, where the squares represent single BChl *c* molecules except for the case of **IV** where they represent dimeric BChl *c* units held together by two strong (Mg···OH) bonds. The connotations i and j represent the two kinds of bonds which hold these entities together to form the two-dimensional sheets; i denoting the presumably stronger and j the presumably weaker of the two. In the cases of **I** and **II**, i equals one (Mg···OH) bond, in the case of **III** one (Mg···OH) plus one hydrogen (C═O···HO) bond, and in the case of **IV** two hydrogen (C═O···HO) bonds. In the cases of **I** and **II**, j equals one hydrogen (C═O···HO) bond, and in the cases of **III** and **IV** it essentially equals two electrostatic (C═O···Mg) bonds plus $\pi-\pi$ interactions. The growth of a sheet such as the one depicted schematically in Figure 15 (general structure) will depend on whether particular BChl *c* molecules, or groups of such molecules, which are attached to the periphery of the sheet, will or will not leave the sheet faster than they become "pinned down" by further molecules that attach to them and to the sheet; obviously, the more bonds to the rest of the sheet a peripheral group has, the more likely it is to stay rather than leave. Thus, there is a "critical" number of bonds to the rest of the sheet that a peripheral group must have in order for it to stay. A single bond i or j (such as exhibited by the bottom molecule in the general structure) is clearly below the critical number, for if it were not, there would be no autocatalysis. (Note that for the sake of simplicity we call the square symbols in the general structure *molecules* even if they are, in the case of **IV**, dimeric.)

The first basic assumption that we make is that a couple of one bond i and one bond j, such as exhibited by the "corner" molecules in the general structure, already fulfills the critical number. Thus, these corner molecules "stay". Since i is stronger than j, it follows that two bonds i also fulfill the critical number; thus the two-molecule group on top of the general structure will stay. We make no assumption on how many bonds j (alone, without any i) are required to fulfill the critical number; we shall call the critical number of j bonds *m*. If we call the vertical edges of the general structure in Figure 15 j-edges (since further molecules will attach to that edge by j bonds) and the horizontal ones i-edges, it follows from the above that the (topological) rectangle (in terms of the general structure in Figure 15) whose i-edge is two molecules long and whose j-edge *m* molecules, constitutes the critical nucleus which has the defining property that it will attach further molecules faster than it will decompose.

The second basic assumption that we make is that most of the dimers and oligomers **L** in the solution are *not partial structures* of **H**; in other words, they have a different architecture.[30] Therefore, every growing sheet, the general structure of which is not a rectangle, will at first tend to complete the rectangle, since only monomer molecules can add "faultlessly" (which follows from the second assumption) and since corner molecules stay.

As shown in the Appendix, these two assumptions lead to the equation

$$[\mathbf{B_H}]\epsilon_{739} = A = f[\mathbf{B_{tot}}]^{(3m/2-1)/g}\, h \exp\{l\,[\mathbf{B_{tot}}]^{(m/2+1)/g}\, t\} + d \tag{26}$$

where $[\mathbf{B_H}]$, $A$, and $[\mathbf{B_{tot}}]$ are as given above (see eqs 2 and 3), $d$ and $h$ are unknown functions of $[\mathbf{B_{tot}}]$ but no functions of $t$; $f$ and $l$ are constant factors and g = 1 in case **IV** and 2 in cases **I**−**III**. Thus, eq 26 is a function both of $[\mathbf{B_{tot}}]$ and of time $t$.

Comparison of eq 26 with eqs 2 and 3 shows the agreement between our kinetic modeling and the experiment. For the exponential term (exp{...$t$} in (eq 26)), the agreement is perfect, whereas for the preexponential term some uncertainty remains since the dependence of $h$ on $[\mathbf{B_{tot}}]$ is not known. Comparison between eqs 26, 2, and 3 within the exponential term shows that

$$2.31 \pm 0.1 = m/2 + 1 \qquad \text{in case } \mathbf{IV}$$

$$2.31 \pm 0.1 = (m/2 + 1)/2 \qquad \text{in cases } \mathbf{I}-\mathbf{III}$$

Hence

$$m = 2.62 \pm 0.2 \text{ in case } \mathbf{IV}$$

$$m = 7.24 \pm 0.4 \text{ in cases } \mathbf{I}-\mathbf{III}$$

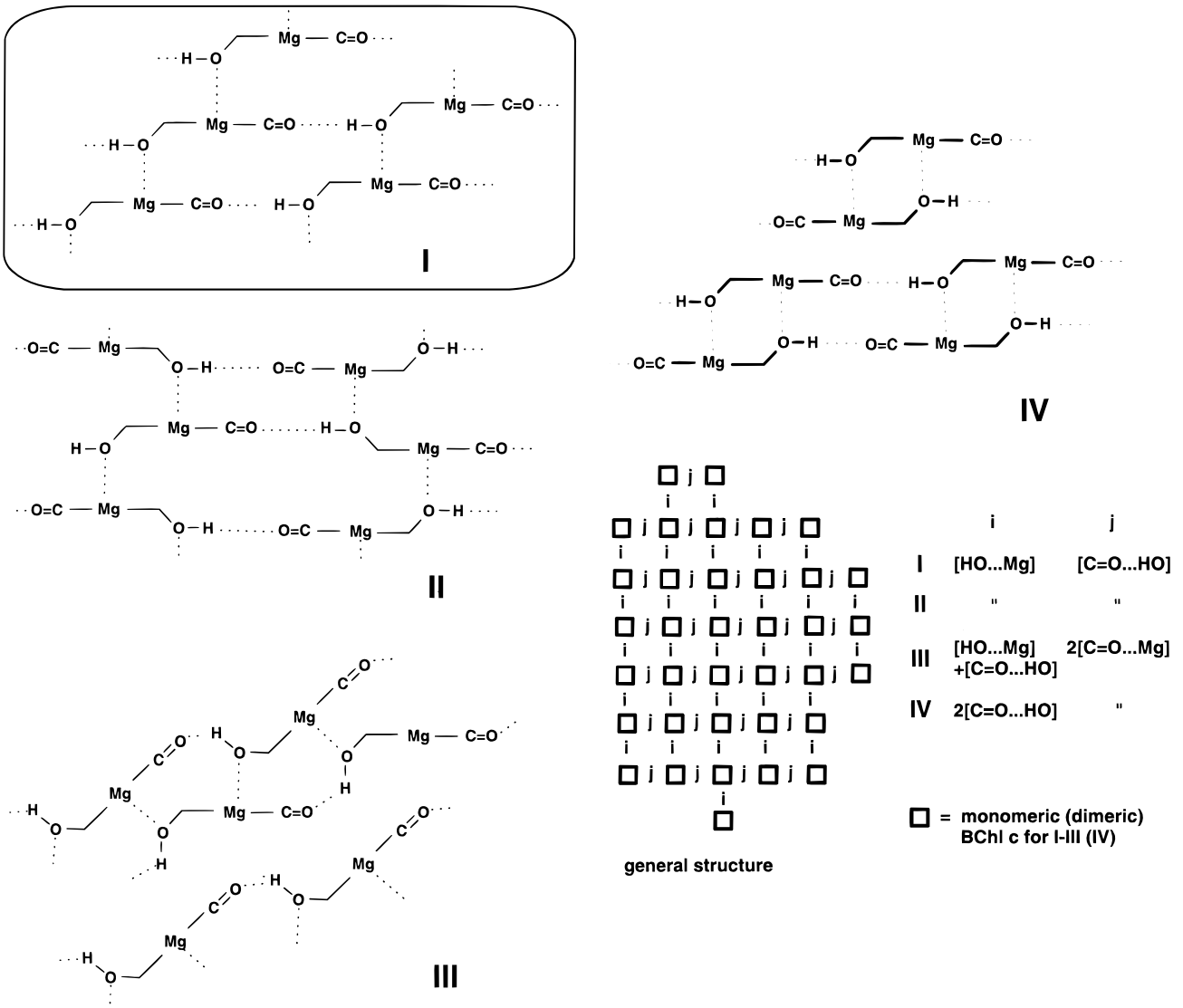


**Figure 15.** Four conceivable architectures (**I**−**IV**) of the two-dimensional sheets in chlorosomal-type aggregates complying with the bonding scheme of Figure 1. All four architectures can be symbolized by a general structure which is also shown, the squares representing BChl *c* units which are monomers in cases **I**−**III** and a dimer held together by two (Mg···OH) bonds in case **IV**. Connotations i and j are the bonds between the units.

Thus, the size of the critical nucleus is 7.2 × 2, i.e., roughly 14, in the cases **I**−**III**, and 2.6 ×2 × 2 (the second factor of 2 is due to the unit being dimeric), i.e., roughly 10, in case **IV**.

We noted above that the slowness of the buildup reaction, as compared to the rapid equilibration between monomer, dimers, and oligomers **L**, suggested that the equilibrium concentration of the critical nucleus must be very low. Since dimers are the prevailing species in the early phases of the buildup, there is little wonder that a 14-mer or 10-mer which, moreover, has an architecture differing from that of **L**, should have such a very low equilibrium concentration.

## Conclusion

Solutions of BChl *c* in $CH_2Cl_2$ contain monomers, dimers, and lower aggregates (**L**). Upon dilution (ca. 1:100) of such solutions with *n*-hexane to BChl *c* concentrations in the 4−50 $\mu$M range these monomers, dimers, and **L** are virtually quantitatively converted into higher, chlorosomal-type aggregates, **H**, characterized by an absorption maximum at 739 nm, which is strongly red-shifted with respect to the maxima of the other species. The absorbance at 739 nm can serve as a quantitative gauge for the concentration (referring to a unit volume of the entire solution/suspension) of BChl *c* that is present in **H**. The buildup of this absorbance after addition of the *n*-hexane in the given concentration range takes minutes to hours until completion and thus can be studied conveniently. It is found to consist of an induction period followed by an exponential growth which then levels off in approach of the final equilibrium state. The experiments show that eqs 2 and 3 describe quantitatively the buildup in time of this absorption during the exponential growth phase. We present a kinetic model for this phase of the aggregation process to **H**, which is based on the two-dimensional sheet structure of **H** (the chlorosomal-type aggregates are tubuli, and thus are curved sheets that have closed to form a tube) and on the assumption (for which there is experimental evidence) that the architectures of **H** and **L** are different. This model thus represents a special kinetic case of two-dimensional crystal growth characterized by a spontaneous formation of a "critical" **H** nucleus (analogous to a crystal nucleus in crystallization) which then grows by attachment of further BChl *c* molecules. This model correctly predicts the form of the eqs 2 and 3. From the parameter values in eqs 2 and 3

and in line with the kinetic model, the critical nucleus is found to be a topological rectangle consisting of approximately 14 BChl *c* molecules for three possible architectures of the sheets including the one that is strongly favored by the available experimental and computational evidence,[12b,13b,16] and of approximately 10 molecules for a fourth (hypothetical) one.

**Acknowledgment.** We thank Manuela Trinoga for technical assistance. Partial financial support by the EU-TMR Program Green Bacterial Photosynthesis and by an award from the Human Frontier Science Organization is gratefully acknowledged.

**Appendix: Derivation of Equation 26**

(Please read first the two paragraphs preceding eq 26 in the text.) If we call the length of the i edge of the rectangle $p$ and the length of the j edge $q$, it follows that the rate of adding a new row to the i edge will be proportional to $[\mathbf{M}]^2(p-1)$, [**M**] being the concentration of monomeric BChl *c* in the cases **I**−**III** and the concentration of the dimeric unit held together by two (Mg···OH) bonds in the case **IV**; analogously, the rate of adding a new row to the j edge will be proportional to $[\mathbf{M}]^m(q-m+1)$. Since the first process will increase $q$ by 1 and the latter process will increase $p$ by 1, we can write

$$\mathrm{d}q/\mathrm{d}t = k_\mathrm{i}[\mathbf{M}]^2(p-1)$$

and

$$\mathrm{d}p/\mathrm{d}t = k_\mathrm{j}[\mathbf{M}]^m(q-m+1)$$

If $p$ and $q$ have already grown to sufficiently large values we can simplify these two equations to give

$$\mathrm{d}q/\mathrm{d}t = k_\mathrm{i}[\mathbf{M}]^2 p \tag{4}$$

and

$$\mathrm{d}p/\mathrm{d}t = k_\mathrm{j}[\mathbf{M}]^m q \tag{5}$$

We note that addition of a new layer on the i edge will increase the propensity to form a new layer on the j edge, while leaving the corresponding propensity for the i edge unchanged, and vice versa. This situation will lead to a quasi-stationary state such that

$$(\mathrm{d}p/\mathrm{d}t)/(\mathrm{d}q/\mathrm{d}t) = p/q \tag{6}$$

if we assume [**M**] to remain constant in the early time regime considered, after the induction period but well before the inflection point. Since the number of molecules contained in a rectangular sheet is $pq$, the rate of growth of that sheet is given by $\mathrm{d}(pq)/\mathrm{d}t$ for which we can write two equations, using eqs 4−6.

$$\mathrm{d}(pq)/\mathrm{d}t = p(\mathrm{d}q/\mathrm{d}t) + (\mathrm{d}p/\mathrm{d}t)q = 2p(\mathrm{d}q/\mathrm{d}t) = 2k_\mathrm{i}[\mathbf{M}]^2p^2 \tag{7}$$

$$\mathrm{d}(pq)/\mathrm{d}t = p(\mathrm{d}q/\mathrm{d}t) + (\mathrm{d}p/\mathrm{d}t)q = 2(\mathrm{d}p/\mathrm{d}t)q = 2k_\mathrm{j}[\mathbf{M}]^m q^2 \tag{8}$$

Since the right-hand sides in eqs 7 and 8 must be equal, they can be replaced by their geometric mean; hence

$$\mathrm{d}(pq)/\mathrm{d}t = 2(k_\mathrm{i}k_\mathrm{j})^{1/2}[\mathbf{M}]^{m/2+1}pq \tag{9}$$

Integration yields

$$p_\mathrm{t}q_\mathrm{t} = p_\mathrm{r}q_\mathrm{r}\exp\{2(k_\mathrm{i}k_\mathrm{j})^{1/2}[\mathbf{M}]^{m/2+1}(t-t_\mathrm{r})\} \tag{10}$$

"$p_tq_t$" refers to a time t after the zero point ($t = 0$) in the lifetime of the sheet which is the point at which buildup started from the nucleus (as defined above), whereas "$p_\mathrm{r}q_\mathrm{r}$" refers to a reference time $t_\mathrm{r}$ which is earlier than $t$ but sufficiently later than the zero point for the quasi-stationary state to be reached and for $p \cong p-1$ and $q \cong q-m+1$ to hold. We can now write for the rate of generation of BChl *c* molecules that are bound in sheets **H** (denoting these BChl *c* molecules by $\mathbf{B_H}$, vide supra):

$$\mathrm{d}[\mathbf{B_H}]/\mathrm{d}t = (\mathrm{d}[\mathbf{H}]/\mathrm{d}t)\,p_tq_t \tag{11}$$

where $\mathrm{d}[\mathbf{H}]/\mathrm{d}t$ is the rate of formation of new sheets, *i.e.*, the rate of spontaneous formation of critical nuclei, and where the index t now refers to the time that has elapsed since the addition of hexane to the $CH_2Cl_2$ solution. (Hint: Within a unit of time, new sheets will be formed and all old ones will grow. This process can be viewed, through a bookkeeper's eye, as though the largest, i.e., the oldest, sheets were formed at once at a rate equivalent to the rate of formation of nuclei, while all other sheets including the nuclei remained unchanged. The quantity $p_tq_t$ then equals the number of BChl *c* molecules in these oldest sheets.)

For $\mathrm{d}[\mathbf{H}]/\mathrm{d}t$ we can write

$$\mathrm{d}[\mathbf{H}]/\mathrm{d}t = k_h[\mathbf{M}]^{2m} \tag{12}$$

(Recall that $2m$ is the size of the critical nucleus.) From eqs 10−12 we obtain

$$\mathrm{d}[\mathbf{B_H}]/\mathrm{d}t = k_h[\mathbf{M}]^{2m}\,p_\mathrm{r}q_\mathrm{r}\exp\{2(k_\mathrm{i}k_\mathrm{j})^{1/2}[\mathbf{M}]^{m/2+1}(t-t_\mathrm{r})\} \tag{13}$$

Integration yields

$$[\mathbf{B_H}] - [\mathbf{B_H}]_\mathrm{r} = rp_\mathrm{r}q_\mathrm{r}\{\exp[s(t-t_\mathrm{r})] - 1\} \tag{14}$$

where

$$r = (k_h/2)\,(k_\mathrm{i}k_\mathrm{j})^{-1/2}[\mathbf{M}]^{3m/2-1} \tag{15}$$

and

$$s = 2(k_\mathrm{i}k_\mathrm{j})^{1/2}[\mathbf{M}]^{m/2+1} \tag{16}$$

Equation 14 can be rearranged to

$$[\mathbf{B_H}] = c'\exp(st) + d' \tag{17}$$

where

$$c' = rp_\mathrm{r}q_\mathrm{r}\exp(-st_\mathrm{r}) \tag{18}$$

and

$$d' = [\mathbf{B_H}]_\mathrm{r} - rp_\mathrm{r}q_\mathrm{r} \tag{19}$$

Both $c'$ and $d'$ are independent of the choice of the reference point, *i.e.*, of $t_\mathrm{r}$, $p_\mathrm{r}q_\mathrm{r}$, and $[\mathbf{B_H}]_\mathrm{r}$. In the case of $c'$, this follows from the fact that both $r$ and the left side in the eq 20 which follows from eqs 10 and 16,

$$p_tq_t\exp(-st) = p_\mathrm{r}q_\mathrm{r}\exp(-st_\mathrm{r}) \tag{20}$$

are independent of the choice of the reference point. In the case of $d'$, this follows from eq 21 which is obtained from eqs 14 and 20,

$$[\mathbf{B_H}] - rp_tq_t = [\mathbf{B_H}]_r - rp_rq_r \qquad (21)$$

since the left side of eq 21 must be independent of the choice of the reference point. The values of $c'$ and $d'$ will, of course, depend on [**M**] in some way.

Equation 17 can be rewritten as

$$[\mathbf{B_H}]\epsilon_{739} = A = c\,\exp(st) + d \qquad (22)$$

where $A$ is now the absorbance of $\mathbf{B_H}$ at 739 nm (as plotted in Figure 4) and $c$ and $d$ are $\epsilon_{739}c'$ and $\epsilon_{739}d'$, respectively, where $\epsilon_{739}$ is the absorption coefficient of $\mathbf{B_H}$ at 739 nm.

We shall now replace the quantity [**M**] in the above expression for $s$, eq 16, by [$\mathbf{B_{tot}}$], i.e., replace the monomer (cases **I**−**III**) or dimer (case **IV**) concentrations by the overall concentration. We noted above that the equilibria between BChl *c* monomers and the various oligomers of type **L** are established rapidly as compared to the slow buildup reaction of the aggregates **H**. To relate [**M**] and [$\mathbf{B_{tot}}$], we can therefore apply equilibrium expressions. From our detailed studies of these equilibria in $CH_2Cl_2$,[32] we can estimate that under our conditions in the initial phases of the buildup reaction the large majority of the BChl *c* molecules will be dimeric. Thus,

$$[\mathbf{Dim}] \cong a[\mathbf{B_{tot}}] \qquad (23)$$

where **Dim** is the sum of dimers of any structure, and a is a roughly constant factor slightly less than unity. In case **IV**, M is a particular dimer (vide supra) the concentration of which will be proportional to [**Dim**]; hence, from eq 23,

$$\text{in case } \mathbf{IV}\text{: } [\mathbf{M}] \cong ab[\mathbf{B_{tot}}] \qquad (24a)$$

where $b$ is a constant less than unity. For cases **I**−**III**, [**M**] is the monomer concentration which is related to [**Dim**] according to $[\mathbf{M}] = (K[\mathbf{Dim}])^{1/2}$ where $K$ is an equilibrium constant. From this and eq 23, in cases **I**−**III**: $[\mathbf{M}] \cong (aK[\mathbf{B_{tot}}])^{1/2}$ (24b).

Introducing eqs 24a and 24b into eq 16 we obtain

$$s = 2(k_ik_j)^{1/2}(ab)^{m/2+1}[\mathbf{B_{tot}}]^{m/2+1} \qquad (25a) \text{ in case } \mathbf{IV}$$

and

$$s = 2(k_ik_j)^{1/2}(a\mathrm{K})^{(m/2+1)/2}[\mathbf{B_{tot}}]^{(m/2+1)/2} \qquad (25b) \text{ in cases } \mathbf{I}-\mathbf{III}$$

respectively.

Considering eqs 15, 18, 19, 24a, 24b, 25a, and 25b, eq 22 becomes

$$[\mathbf{B_H}]\,\epsilon_{739} = A = f\,[\mathbf{B_{tot}}]^{(3m/2-1)/g}\,h\,\exp\{l\,[\mathbf{B_{tot}}]^{(m/2+1)/g}\,t\} + d \qquad (26)$$

where $f = (\epsilon_{739})\,(k_h/2)\,(k_ik_j)^{-1/2}(ab)^{3m/2-1}$ in case **IV**, and $f = (\epsilon_{739})\,(k_h/2)\,(k_ik_j)^{-1/2}(a\mathrm{K})^{(3m/2-1)/2}$ in cases **I**−**III** (thus, $f$ is a constant factor); $g = 1$ in case **IV** and 2 in cases **I**−**III**; $h = p_rq_r\exp(-st_r)$, i.e., an unknown function of [$\mathbf{B_{tot}}$] but no function of $t$ (vide supra); $l = 2(k_ik_j)^{1/2}(ab)^{m/2+1}$ in case **IV**, and $l = 2(k_ik_j)^{1/2}(a\mathrm{K})^{(m/2+1)/2}$ in cases **I**−**III** (thus, $l$ is a constant factor); and $d = (\epsilon_{739})\,([\mathbf{B_H}]_r - rp_rq_r)$; i.e., an unknown function of [$\mathbf{B_{tot}}$] but no function of $t$ (vide supra)

## References and Notes


(1) Lehn, J.-M. *Supramolecular Chemistry*. *Concepts and Perspectives*; VCH: Weinheim, 1995.

(2) (a) Lawrence, D. S.; Jiang, T.; Levett, M. *Chem. Rev.* **1995**, *95*, 2229. (b) Amabilino, D. B.; Stoddart, J. F. *Chem. Rev.* **1995**, *95*, 2725. (c) Gillard, R. E.; Raymo, F. M.; Stoddard, J. F. *Chem. Eur. J.* **1997**, *3*, 1933. (d) Philp, D.; Stoddard, J. F. *Angew. Chem.* **1996**, *108*, 1242; *Angew. Chem., Int. Ed. Engl.* **1996**, *35*, 1154.

(3) Abbreviations: BChl *c*, ($3^1R$)-[Et,Et] bacteriochlorophyll $c_F$ (prescript such as [Et,Et] refers to substituents at C-8 and C-12; subscripts F and S, farnesyl and stearyl, respectively). [$\mathbf{B_{tot}}$], overall concentration ($\mu$M) of BChl *c*. [**M**], concentration of monomeric BChl *c*. [**Dim**], concentration of all kinds of dimeric BChl *c*. **L**, low molecular BChl *c* oligomers as prevailing in $CH_2Cl_2$ solutions. **H**, chlorosomal-type BChl *c* aggregates and sheets of BChl *c* molecules that represent parts of these aggregates. [$\mathbf{B_H}$], concentration of BChl *c* (with respect to the total solution/suspension) contained in **H**.

(4) (a) Smith, K. M.; Craig, C. W.; Kehres, L. A.; Pfennig, N. *J. Chromatogr.* **1983**, *281*, 209. (b) Fages, F.; Griebenow, N.; Griebenow, K.; Holzwarth, A. R.; Schaffner, K. *J. Chem. Soc., Perkin Trans. 1* **1990**, 2791.

(5) For reviews see (a) Olson, J. M. *Photochem. Photobiol.* **1998**, *67*, 61. (b) Blankenship, R. E.; Olson, J. M.; Miller, M. In *Anoxygenic Photosynthetic Bacteria*; Blankenship, R. E., Madigan, M. T., Bauer, C. E., Eds.; Kluwer Academic Publishers: Dordrecht, 1995; pp 399−435. (c) Holzwarth, A. R.; Griebenow, K.; Schaffner, K. *J. Photochem. Photobiol A: Chem.* **1992**, *65*, 61.

(6) (a) McDermott, G.; Prince, S. M.; Freer, A. A.; Hawthornthwaite-Lawless, A. M.; Papiz, M. Z.; Cogdell, R. J.; Isaacs, N. W. *Nature* **1995**, *374*, 517. (b) Koepke, J.; Hu, X.; Muenke, C.; Schulten, K.; Michel, H. *Structure* **1996**, *4*, 581.

(7) (a) Bystrova, M. I.; Mal'gosheva, I. N.; Krasnovskii, A. A. *Mol. Biol. Engl. Transl.* **1979**, *13*, 440. (b) Smith, K. M.; Kehres, L. A.; Fajer, J. *J. Am. Chem. Soc.* **1983**, *105*, 1387.

(8) (a) Mimuro, M.; Nozawa, T.; Tamai, N.; Shimada, K.; Yamasaki, I.; Lin. S.; Knox, R. S.; Wittmershaus, B. P.; Brune, D. C.; Blankenship, R. E. *J. Phys. Chem.* **1989**, *93*, 7503. (b) Hirota, M.; Morijama, T.; Shimada, K.; Miller, M.; Olson, J. M.; Matsuura, K. *Biochim. Biophys. Acta*, **1992**, *1099*, 271.

(9) (a) Holzwarth, A. R.; Müller, M. G.; Griebenow, K. *J. Photochem. Photobiol. B: Biol.* **1990**, *5*, 457. (b) Causgrove, T. P.; Brune, D. C.; Blankenship, R. E.; Olson, J. M. *Photosynth. Res.* **1990**, *25*, 1. (c) Savikhin, S.; van Noort, P. I.; Blankenship, R. E.; Struve, W. S. *Biophys. J.* **1995**, *69*, 1100.

(10) (a) Brune, D. C.; Nozawa, T.; Blankenship, R. E. *Biochemistry* **1987**, *26*, 8644. (b) Brune, D. C.; Gerola, P. D.; Olson, J. M. *Photosynth. Res.* **1990**, *24*, 253. (c) Balaban, T. S.; Holzwarth, A. R.; Schaffner, K. *J. Mol. Struct.* **1995**, *349*, 183.

(11) Hildebrandt, P.; Tamiaki, H.; Holzwarth, A. R.; Schaffner, K. *J. Phys. Chem.* **1994**, *98*, 2192.

(12) (a) Uehara, K.; Ozaki, Y.; Okada, K.; Olson, J. M. *Chem. Lett.* **1991**, 909. (b) Chiefari, J.; Griebenow, K.; Fages, F.; Griebenow, N.; Balaban, T. S.; Holzwarth, A. R.; Schaffner, K. *J. Phys. Chem.* **1995**, *99*, 1357.

(13) (a) Nozawa, T.; Ohtomo, K.; Suzuki, M.; Nakagawa, H.; Shikama, Y.; Konami, H.; Wang, Z.-Y. *Photosynth. Res.* **1994**, *41*, 211. (b) Balaban, T. S.; Holzwarth, A. R.; Schaffner, K.; Boender, G. J.; de Groot, H. J. M. *Biochemistry*, **1995**, *34*, 15259. (c) van Rossum, B.-J.; Boender, G. J.; Mulder, F. M.; Raap, J., Balaban, T. S.; Holzwarth, A. R.; Schaffner, K.; Prytulla, S.; Oschkinat, H.; de. Groot, H. J. M. *Spectrochim. Acta* **1998**, *A51*, 1167.

(14) (a) Worcester, D. L.; Michalski, T. J.; Katz, J. J. *Proc. Natl. Acad. Sci. U.S.A.* **1986**, *83*, 3791. (b) Worcester, D. L.; Michalski, T. J.; Bowman, M. K.; Katz, J. J. *Mater. Res. Soc. Symp. Proc.* **1990**, *174*, 157.

(15) Staehelin, L. A.; Golecki, J. R.; Fuller, R. C.; Drews, G. *Arch. Mikrobiol.* **1978**, *119*, 269.

(16) Holzwarth, A. R.; Schaffner, K. *Photosynth. Res.* **1994**, *41*, 225.

(17) (a) Mizoguchi, T.; Sakamoto, S.; Koyama, Y.; Ogura, K.; Inagaki, F. *Photochem. Photobiol.* **1998**, *67*, 239. (b) Mizoguchi, T.; Matsuura, K.; Shimada, K.; Koyama, Y. *Chem. Phys. Lett.* **1996**, *260*, 153. (c) Mizoguchi, T.; Limantara, L.; Matsuura, K.; Shimada, K.; Koyama, Y. *J. Mol. Struct.* **1996**, *379*, 249.

(18) (a) Olson, J. M.; Pedersen, J. P. *Photosynth. Res.* **1990**, *25*, 25. (b) Olson, J. M.; Pedersen, J. P.; Causgrove, T. P.; Brune, D. C.; Blankenship. R. E. In *Current Research in Photosynthesis*; Baltscheffsky, M., Ed.; Kluwer Academic Publishers: Dordrecht, 1990; Vol II, p 37. (c) Olson, J. M.; Cox, R. P. *Photosynth. Res.* **1991**, *30*, 35.

(19) (a) Hirota, M.; Moriyama, T.; Shimada, K.; Miller, M.; Olson, J. M.; Matsuura, K. *Biochim. Biophys. Acta* **1992**, *1099*, 271. (b) Miller, M.; Gillbro, T.; Olson, J. M. *Photochem. Photobiol.* **1993**, *57*, 98.

(20) Dudkowiak, A.; Francke, C.; Amesz, J. *Photosynth. Res.* **1996**, *46*, 427.

(21) For extensive studies of the response of chlorosomal BChl *c* aggregates in buffers to *n*-hexanol, see (a) Matsuura, K.; Olson, J. M.; *Biochim. Biophys. Acta* **1990**, *1019*, 233. (b) Zhu, Y.; Ramakrishna, B. L.; van Noort, P. I.; Blankenship, R. E. *Biochim. Biophys. Acta* **1995**, *1232*, 197. (c) Wang, Z.-Y.; Marx, G.; Umetsu, M.; Kobayashi, M.; Mimuro, M.; Nozawa, T. *Biochim. Biophys. Acta* **1995**, *1232*, 187.

(22) Van Brakel, G. H.; Olson, J. M. Unpublished work cited in ref 15a.

(23) High vapor pressure is a technical disadvantage of $CH_2Cl_2$. It renders quantitative manipulations of small volumes of solutions and absorption measurements in thin (0.1 mm) cuvettes difficult. $C_2H_2Cl_4$ overcomes this drawback and is an excellent solvent for BChl *c*. The same species are formed when experimenting with stock solutions of both solvents. This has been ascertained by comparison of the absorption spectra under all relevant conditions described in detail for the case of $CH_2Cl_2$.

(24) Eaton, W. A.; Hofrichter, J. *Adv. Prot. Chem.* **1990**, *40*, 63.

(25) de Paula, J. C.; Roblee, J. H.; Pasternack, R. F. *Biophys. J.* **1995**, *68*, 335.

(26) Pasternack, R. F.; Gibbs, E. J.; Collings, P. J.; de Paula, J. C.; Turzo, L. C.; Terracina, A. *J. Am. Chem. Soc.* **1998**, *120*, 5873.

(27) Oxtoby, D. W. *Acc. Chem. Res.*, **1998,** *31*, 91.

(28) This represents an example of the repair mechanism that is common with self-assembly processes that involve reversible steps.[1,2]

(29) Brune, D. C.; King, G. H.; Blankenship, R. E. In *Photosynthetic Light-Harvesting Systems*; Scheer, H., Schneider, S., Eds.; Walter de Gruyter: Berlin, 1988; pp 141−151.

(30) It is now established that the oligomers **L** are related to architecture **IV** in Figure 15: The basic unit of **L** is the unsymmetric version of the dimer from which **IV** is built.[31] This dimer is stable on the NMR time scale and is in rapid (on the NMR time scale) equilibrium with its oligomeric aggregates.[18] **H**, however, possesses architecture **I** in Figure 15 (vide supra), hence our assumption.

(31) Wang, Zh.-Y.; Umetsu, M.; Kobayashi, M.; Nozawa, T. *J. Phys. Chem. B* **1999**, *103*, 3742.

(32) Balaban, T. S., Leitich, J., Holzwarth, A. R., Schaffner, K. In preparation.